Int. J. Nonlinear Anal. Appl. 15 (2024) 5, 91–102
ISSN: 2008-6822 (electronic)
http://dx.doi.org/10.22075/ijnaa.2022.27790.3713

Selecting the most efficient cross-sectional configuration of a multi-cell hexagonal tube under axial dynamic loading based on crashworthiness performance criteria

Reza Sistani, Mahmoud Mousavi Mashhadi*, Younes Mohammadi

Department of Mechanical Engineering, Faculty of Industrial and Mechanical Engineering, Qazvin Branch, Islamic Azad university, Qazvin, Iran

(Communicated by Farshid Khojasteh)

Abstract

The purpose of this paper is to select the optimal section of different cross-sectional multi-cell hexagonal tubes under axial dynamic loads in three categories of internal edge thicknesses. The explicit non-linear FE code LS-DYNA is employed for numerical simulation. The results of crashworthiness performance criteria are obtained for various alternatives of configurations. TOPSIS method introduces the rank of different sections. The most effective section in the three categories is selected. In the continuation of the research, the straight inner sides of small hexagons were replaced with semi-elliptic and semicircle, but with respect to the symmetry of the larger hexagon diameter and equal perimeter size in order to evaluate the crashworthiness criteria in the selected section.

Keywords: Dynamic axial load, crashworthiness criteria, multi-cell hexagonal tube, specific energy absorption, peak force, TOPSIS method
2020 MSC: 70Q05, 74H05

1 Introduction

Crashworthiness is a vital element in designing vehicle structures because the huge kinematic energy generated during the collision cannot be dissipated in time [6]. Higher energy absorption efficiency and better crashworthiness performance are the primary objectives for energy-absorbing structures in the railroad, aerospace, offshore, and automotive industries, among others [9]. Numerous studies have been conducted to enhance vehicle crashworthiness and reduce passenger injury and fatality rates [27]. Metal thin-walled structures, such as multi-cell columns, have been extensively applied in crashworthy components to dissipate the kinetic energy in a collision. Similarly, many studies have investigated the crashworthiness of multi-cell tubes [1, 2, 14, 20, 21]. Aluminum alloys are gaining a favorable reputation due to their lightness and ductility, and they can be produced in almost any shape using the extrusion process [16].

McFarland determined the approximate crushing stress of hexagonal cell structures subjected to axial loading [7]. Wierzbicki proposed a simple method based on energy consideration in conjunction with a minimum principle in plasticity for the mean crushing force of hexagonal structures [17]. Zhang derived analytic formulas for the average

*Corresponding author
Email addresses: rezasistani@gmail.com (Reza Sistani), mmosavi@qiau.ac.ir (Mahmoud Mousavi Mashhadi), u.mohammadi@gmail.com (Younes Mohammadi)

Received: April 2022 *Accepted:* July 2022

crushing force for two, three, and four panels and calculated and combined several multi-cell square columns using these formulas. He validated these theoretical solutions with numerical and experimental methods [19, 22, 24, 25, 23, 26]. Wu and Jiang focused on investigating the crushing phenomena of honeycomb structures under quasi-static and dynamic loading [18]. Qiu et al. studied the improved crashworthiness indicators with varying multi-cell hexagonal tubes under axial dynamic loads [10, 12]. Hou proposed that strain rate does not have much influence on an aluminum alloy so it can be neglected, and the dynamic coefficient can be introduced to consider the inertia effect [5, 15].

This paper uses an analytic formulation based on the super folding element method to validate a numerical model of a single hexagonal tube with certain width and thickness under dynamic axial load. The crashworthiness indicators were improved by adding six small hexagonal tubes (complete or in parts). The small internal hexagons have constant width, but their thicknesses are increased in three categories. A multi-criteria decision-making MCDM process was carried out to select the best configuration for each category. A summary and the extracted conclusions are presented at the end of the paper.

2 Preliminaries

2.1 Problem description

2.1.1 Definition of crashworthiness indicators

The total energy absorption E in a crash is equal to the area under the load-displacement curve and is defined as follows.

$$E = \int_0^{Lc} F(i)dx \tag{2.1}$$

where $F(x)$ denotes the instantaneous crushing force in the axial direction, and Lc is the crash distance. It is related to how much energy a structure can absorb to its mass-specific energy absorption obtained. It is defined as:

$$SEA = \frac{E}{m} \tag{2.2}$$

The peak load is the maximum load needed to start the deformation of the structure permanently. The F_{max} that occurs during the crash should not exceed certain criteria. The mean crash force is defined as:

$$F_{mean} = \frac{E}{Lc} \tag{2.3}$$

The crushing force efficiency (CFE) is the ratio between the mean and peak crushing forces, defined as follows:

$$CFE = \frac{F_{mean}}{F_{max}} \times 100 \tag{2.4}$$

The ideal energy absorber would have a CFE value close to 100% because an ideal absorber must preserve a peak load for its entire crushed length. In general, a good crashworthiness design must have a reasonable peak load, a high specific energy absorption, and a CFE value close to 100%.

2.2 Geometrical description

This study introduces a regular hexagonal tube with a certain side size of A=48 (mm), a constant thickness of t_1=1.6 (mm), and a total length of L=180 (mm). This structure is reinforced by adding small hexagonal and sub-hexagonal tubes. These small hexagonal tubes have a side size of B=10 (mm) and different thicknesses in three categories (t_2 = 0.4, 0.6, and 0.8mm). Figure 1 shows different configurations (S_1 - S_7).

3 Numerical analysis

3.1 Finite element analysis

The numerical analyses were carried out using nonlinear explicit code LS-DYNA. Figure 2 shows boundary and impact conditions used in the simulations.

The end of the structures is fully fixed in all directions. The striker, with a mass of 600 (kg) and a velocity of 15 (m/s), crushes the different reinforced hexagonal tubes (S_1 - S_7). The multi-cell column is made of aluminum extrusion

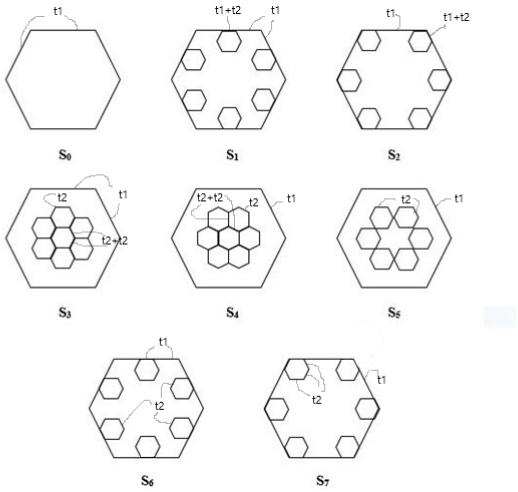

Figure 1: Different design sections of multi-cell hexagonal tubes

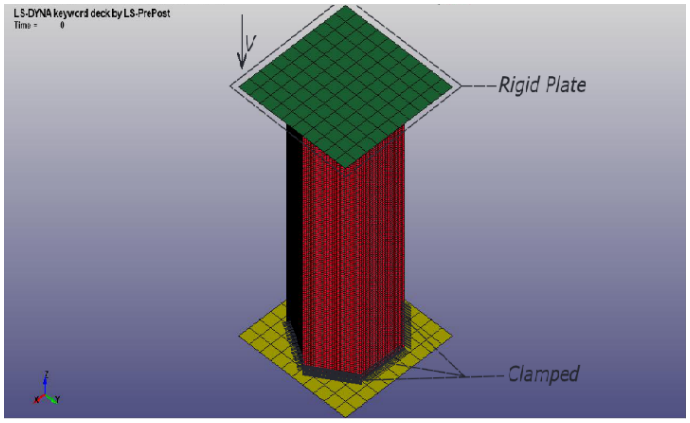

Figure 2: Finite element for axial impact analysis

AA 6061 with these mechanical properties [14]: density ρ =2700 (Kg/m3), Poisson's ratio v=0.33, Young's modulus E=68 (GPa), ultimate stress σ_u=130.7 (Mpa), yield stress σ_y=71(Mpa), and strain hardening exponent n=0.18. The aluminum alloy was modeled using an elastoplastic material model 123 in LS-DYNA [24, 12, 4].

The model was established using Belytschko-Lin-Tsay four-node shell elements with five integration points along the thickness direction. The characteristic size of the mesh is 1.5 (mm) for all configuration tubes. The automatic node-to-surface contact was employed to simulate the interfaces between the tube and striker and between the tube and rigid base. The contacts between the column walls (with and without ribs) and inner walls were defined as automatic single-surface contacts to avoid interpenetration during the crash [10, 12].

Hourglass control, an effective indicator for measuring the reliability of numerical simulation outcomes, was employed to avoid fake zero energy deformation modes (Figure 3).

3.2 Validation of the FE model

The analytical solution of the mean crushing force of a single hexagonal tube under axial dynamic impact has a reasonable agreement with finite element simulation and experimental tests. According to Zhang [24] and Qiu [12], the theoretical formula of the mean crush force for the single hexagonal tube under axial dynamic load is determined as follows:

$$F_{(mean-dynamic)} = \lambda \frac{13.6037}{k} \sigma_0 A^{0.2} t_1^{1.8} \tag{3.1}$$

where A=48 (mm) is the length of width hexagonal tube, t_1= 1.6 (mm) is the wall thickness of the tube, and σ_0 denotes the flow stress of tube material. This paper uses the commonly used explanation to calculate flow stress, as follows.

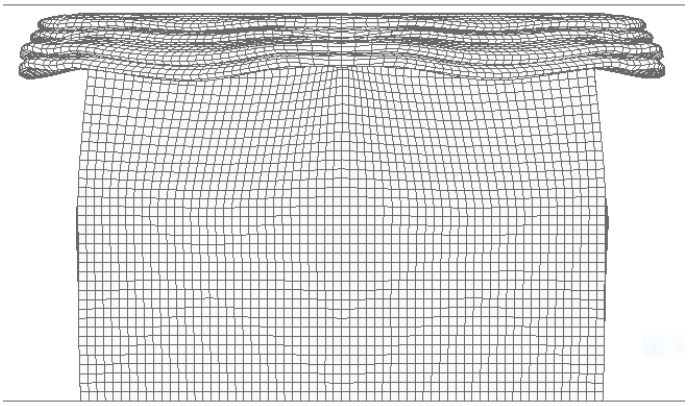

Figure 3: Deformation mode for single hexagonal tube S_0 under dynamic axial load in displacement d=120 (mm)

$$\sigma_0 = \frac{\sigma_u + \sigma_y}{2} \tag{3.2}$$

So, σ_0 = 100.85 (Mpa) [12, 11].

The coefficient K is the ratio of the effective crash distance to the initial length and is calculated as K= 0.74 for a single-wall tube in this validation study. The strain rate does not have much effect on aluminum alloy and can be neglected. Therefore, the dynamic coefficient λ is defined to impose the inertia effect. It ranges from 1.1 to 1.6 and is set at $\lambda = 1.1$ in the present study [12, 5, 15, 3]. Based on the above equation, the average reaction force for a single hexagonal tube was 10.31 (KN), and the mean force from the finite element model was 10.58 (KN). The relative error between the finite element model and the analytical solution of average force was approximately 2.6%. The proposed finite element model in this study is remarkably accurate for further comparative analyses of different configurations under dynamic axial loading.

3.3 Comparison of crashworthiness in different multi-cell tubes under axial dynamic load

Crashing responses of the eight different sectional tubes with three different thicknesses for smaller t_2=0.4 (mm), 0.6 (mm), 0.8 (mm) are obtained under dynamic axial loads by numerical simulation. The results are classified in Tables 1, 2, and 3. Progressive folding and relative curves for these different thicknesses and configurations are shown in Figures 4, 5, and 6.

Table 1: Crash responses of different configurations (t_2=0.4 mm) and decision matrix

	Crashworthiness indicators		
Configuration	SEA (kJ/kg)	F_{max} (KN)	CFE (%)
$S_\emptyset$	5.67	37.46	28.2
S_1	6.51	39.67	40.2
S_2	6.51	41.57	38.4
S_3	6.00	39.11	37.5
S_4	6.00	39.11	37.5
S_5	5.97	38.98	37.5
S_6	6.62	37.80	41.2
S_7	6.35	37.86	37.8

4 Comparison of section designs with different thicknesses of thin-wall tubes based on crashworthiness criteria

The best configuration with multi-criteria for each thickness was selected using the well-known technique for order preference by similarity to the ideal solution (TOPSIS) for multiple-criteria decision analysis. This technique considers

Table 2: Crash responses of different configurations (t_2=0.6 mm) and decision matrix

Configuration	Crashworthiness indicators		
	SEA (kJ/kg)	F_{max} (KN)	CFE (%)
$S_\emptyset$	5.67	37.46	28.2
S_1	7.15	47.29	41.4
S_2	7.61	45.31	46.0
S_3	6.50	49.44	36.1
S_4	6.50	49.44	36.1
S_5	6.54	49.56	36.2
S_6	7.26	43.90	42.9
S_7	7.30	41.25	43.3

Table 3: Crash responses of different configurations (t_2=0.8 mm) and decision matrix

Configuration	Crashworthiness indicators		
	SEA (kJ/kg)	F_{max} (KN)	CFE (%)
$S_\emptyset$	5.67	37.46	28.2
S_1	7.96	53.60	45.0
S_2	8.91	51.48	52.5
S_3	7.10	55.87	40.7
S_4	7.10	55.57	40.7
S_5	7.09	54.49	39.5
S_6	8.50	48.68	49.5
S_7	9.14	46.08	52.4

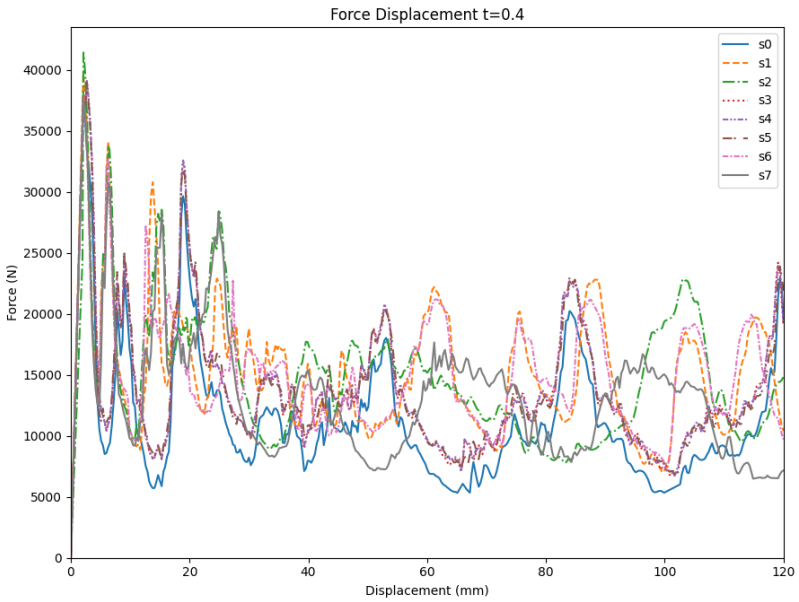

Figure 4: Crushing force–displacement curve for different sectional configuration tubes (S_0-S_7) with the thickness of internal edges t_2= 0.4 (mm)

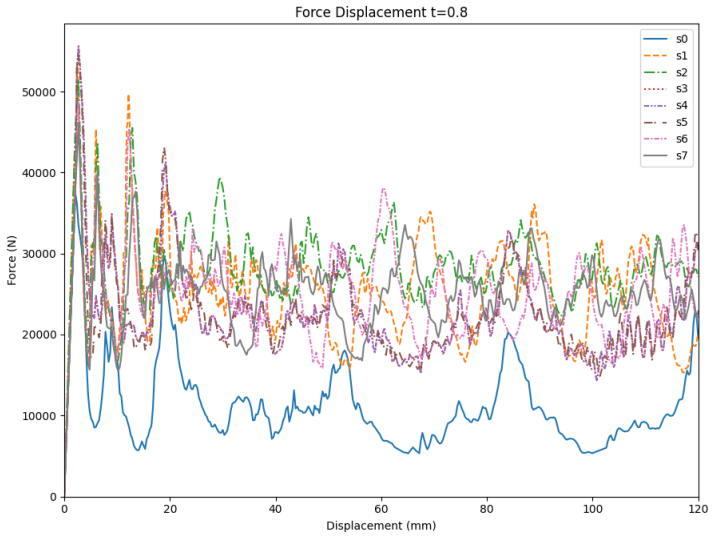

Figure 5: Crushing force–displacement curve for different sectional configuration tubes (S_0-S_7) with the thickness of internal edges t_2= 0.6 (mm)

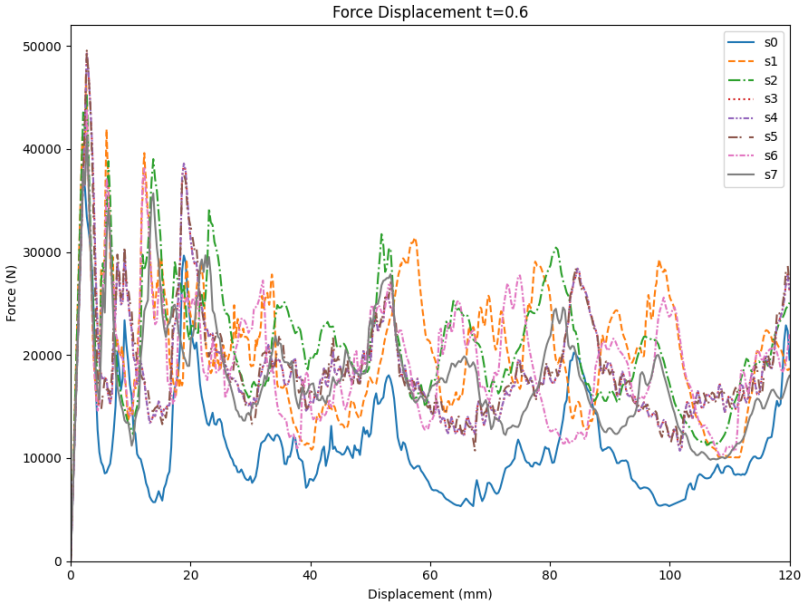

Figure 6: Crushing force–displacement curve for different sectional configuration tubes (S_0-S_7) with the thickness of internal edges t_2= 0.8 (mm)

the distance of each alternative from both the positive-ideal and negative-ideal points [8]. The weight ratios for SEA, F_{max}, and CFE were derived from the AHP method [13] and set at 0.540, 0.297, and 0.163, respectively. This method calculates ratio scales from paired comparisons of criteria. In this study, it is assumed that SEA is more important than F_{max}, and CEF is less important than F_{max}. Tables 4, 5, and 6 show the decision matrices.

4.1 Technique for order preference by similarity to ideal solution (TOPSIS)

The TOPSIS procedure is described in five steps [8].

Step 1. The decision matrix is normalized by the following equation.

Table 4: The weighted normalized decision matrix t_2= 0.4 (mm)

Configuration	SEA	F_{max}	CFE
$S_{\emptyset}$	0.185411	0.107987	0.046374
S_1	0.212879	0.114349	0.066108
S_2	0.212879	0.119825	0.063148
$S_{3,4}$	0196202	0.112734	0.061668
S_5	0.195221	0.112360	0.061668
S_6	0.216476	0.108958	0.067752
S_7	0.207647	0.109131	0.062161

Table 5: The weighted normalized decision matrix t_2= 0.6 (mm)

Configuration	SEA	F_{max}	CEF
$S_{\emptyset}$	0.167986	0.093292	0.043918
S_1	0.211835	0.117773	0.064476
S_2	0.225463	0.112842	0.071640
$S_{3,4}$	0.142577	0.123127	0.056221
S_5	0.193762	0.123426	0.056377
S_6	0.215094	0.109330	0.668121
S_7	0.216279	0.102731	0.067435

Table 6: The weighted normalized decision matrix t_2= 0.8 (mm)

configuration	SEA	F_{max}	CEF
$S_{\emptyset}$	0.148743	0.084098	0.038863
S_1	0.208817	0.120300	0.062015
S_2	0.222146	0.115542	0.072351
$S_{3,4}$	0.186257	0.125395	0.056089
S_5	0.185994	0.122297	0.054436
S_6	0.222983	0.109257	0.068217
S_7	0.239773	0.103422	0.072214

$$V_{i,\,j}\,(x) = \frac{x_{i,\,j}}{\sqrt{\sum_{i=1}^{m} \mathrm{x}_{ij}^2}} \qquad i = 1, ..., m \qquad j = 1, ..., n \tag{4.1}$$

where m and n are the numbers of design alternatives and criteria, respectively.

Step 2. The weighted normalized decision matrix is calculated as follows.

$$V_{i,\,j}\,(x) = W_i\, r_{ij} \qquad i = 1, ..., m \qquad j = 1, ..., n \tag{4.2}$$

Step 3. The positive and negative ideal solutions are determined using the following equations.

$$A^{+} = (V_1^{+}\,,\, V_2^{+}\,, ...,\, V_n^{+}) \tag{4.3}$$

$$A^{-} = (V_1^{-}\,,\, V_2^{-}\,, ...,\, V_n^{-}) \tag{4.4}$$

So that:

$$V_j^{+} = \{(max\, V_{i\,j}(x) \mid j \in j_1), (min\, V_{i\,j}(x) \mid j \in j_2)\} \qquad i = 1, ..., m \tag{4.5}$$

$$V_j^- = \{(min\, V_{i\,j}(x) \mid j \in j_1), (max\, V_{i\,j}(x) \mid j \in j_2)\} \qquad i = 1, ..., m \tag{4.6}$$

where j_1 and j_2 denote the negative and positive criteria.

Step 4. The distances between each alternative and the positive and negative ideal solutions are calculated using the following equations.

$$d_i^+ = \sqrt{\sum_{j=1}^{n} [V_{ij}(x) - V_j^+]^2} \qquad i = 1, ..., m \tag{4.7}$$

$$d_i^- = \sqrt{\sum_{j=1}^{n} [V_{ij}(x) - V_j^-]^2} \qquad i = 1, ..., m \tag{4.8}$$

Step 5. The degree of relative closeness of each alternative to the ideal solution is obtained by following equation.

$$C_i = \frac{d_j^-}{d_i^+ + d_i^-} \qquad i = 1, ..., m \tag{4.9}$$

If the relative closeness degree is near 1, the alternative has a shorter distance from the positive ideal solution and a longer distance from the negative ideal solution.

The results of the TOPSIS method, including the rank of sections, are shown in Tables 7, 8, and 9.

Table 7: Results of TOPSIS method for t_2= 0.4 (mm)

Section	d_i^+	d_i^-	C_i	Rank
$S_\emptyset$	0.037710	0.011847	0.239056	7
S_1	0.007498	0.34262	0.820447	2
S_2	0.013209	0.032184	0.709004	4
$S_{3,4}$	0.021695	0.020015	0.479865	5
S_5	0.022538	0.019643	0.465680	6
S_6	0.00980	0.039245	0.975635	1
S_7	0.010514	0.029292	0.735871	3
The best choice is S_6				

The best answer vector is [0.216476, 0.107978, 0.067752], and the worst answer vector is [0.185411, 0.119825, 0.046374].

Table 8: Results of TOPSIS method for t_2= 0.6 (mm)

Section	d_i^+	d_i^-	C_i	Rank
$S_\emptyset$	0.063812	0.030134	0.320758	7
S_1	0.02892	0.048757	0.627686	4
S_2	0.014550	0.064684	0.767910	2
$S_{3,4}$	0.047004	0.027498	0.369093	6
S_5	0.046324	0.028629	0.381954	5
S_6	0.019699	0.054239	0.733571	3
S_7	0.013824	0.057563	0.806341	1
The best choice is S_7				

The best answer vector is [0.005463, 0.093292, 0.071640], and the worst answer vector is [0.167986, 0.123426, 0.043918].

The best answer vector is [0.239773, 0.084098, 0.072351], and the worst answer vector is [0.148743, 0.125395, 0.038863].

Table 9: Results of TOPSIS method for t_2= 0.8 (mm)

Section	d_i^+	d_i^-	C_i	Rank
$S_\emptyset$ 0.096994	0.041297	0.298623	7	
S_1	0.048740	0.064582	0.569896	4
S_2	0.036023	0.081326	0.693027	3
$S_{3,4}$	0.069526	0.041280	0.372542	5
S_5	0.068354	0.040494	0.3720228	6
S_6	0.030528	0.081447	0.727365	2
S_7	0.019324	0.099405	0.837237	1
The best choice is S_7				

The research continues as follows. Four straight inner edges in the sectional of small hexagonal tubes are replaced with half-elliptical $S_7$1 and semicircle $S_7$2 edges in the final section selected (S_7). The length of the inner straight edges of the small hexagons is set as equal to the circumference of the half elliptical and semicircle. The large radius of the semi-elliptical $S_7$1 is assumed to be 5 (mm) because the circumference of the half-elliptical must be 10 (mm). It can be concluded that the small radius must equal 1.3662 (mm). By reducing the bigger radius of the half-elliptical and increasing the smaller radius of the semi-elliptical section to make them equal, the half-elliptic becomes a semicircle, and the radius of the semicircle is 3.1831 mm) for the $S_7$2 section.

The symmetry of the main hexagonal tube diameters is maintained for all edges (Figure 7). The results of crashworthiness criteria for two different sectional multi-cell tubes ($S_7$1, $S_7$2) under axial dynamic load are obtained by LS-DYNA software, shown in the diagram of force-displacement response in Figure 8.

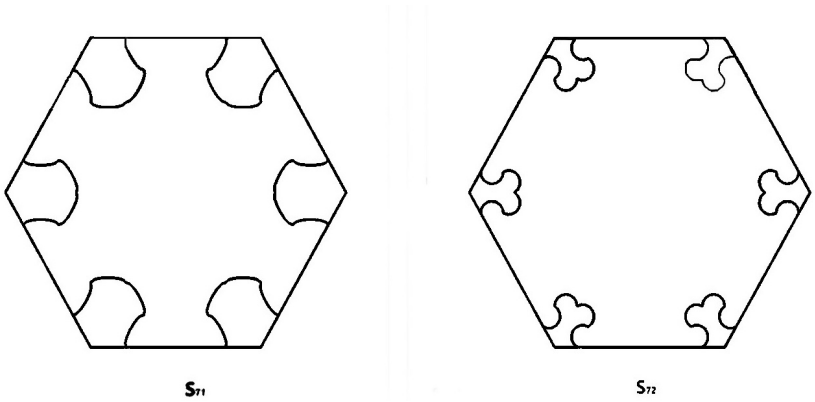

Figure 7: The selected section of multi-cell hexagonal tube with semi-elliptical edges $S_7$1 and semicircle edge $S_7$2

As can be seen in Figure 8, the minimum response force points and the area below the diagram have been further reduced in the $S_7$1 section compared to S_7 and in the $S_7$2 section compared to $S_7$1. In the $S_7$2 section, the minimum response force point from the length of about 60 (mm) strangely decreases when observing the top view and line mode due to the lack of enough space for folding. The results show that the peak force for sections $S_7$1 and $S_7$2 are the same and equal to 47.3 (KN). This value is more than the peak force of section S_7 by 1.2 (KN).

The value of the specific energy absorption for $S_7$1 is 8.43 (KJ/Kg), and for the $S_7$2 section is 7.23 (KJ/Kg), as shown in Figure 9.

The simulation results of collision by LS-DYNA indicate that the new configuration sections ($S_7$1, $S_7$2) are not recommended because, in addition to increased peak force, the SEA decreased with increasing the curvature of straight edges.

5 Conclusion

In this study, a single hexagonal tube with certain and constant outer side width and thickness was reinforced by different arrangements of six small hexagonal tubes (complete or partly) (Figure 1) with certain side widths and different thicknesses (t=0.4, 0.6, 0.8 (mm)) under dynamic axial load. The finite element model was constructed based

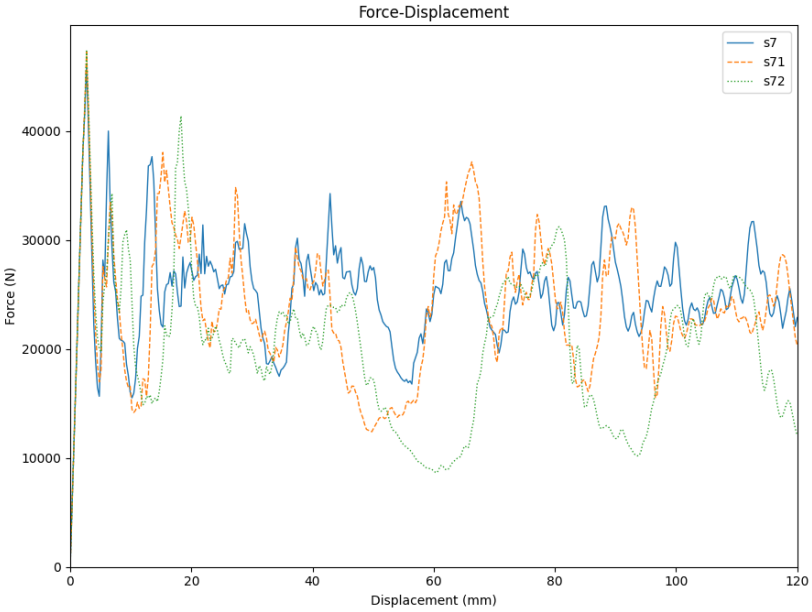

Figure 8: Crushing force-displacement curve for different sectional configuration tubes (S_7, S_71, and S_72) with the thickness of internal ribs t_2=0.8 (mm)

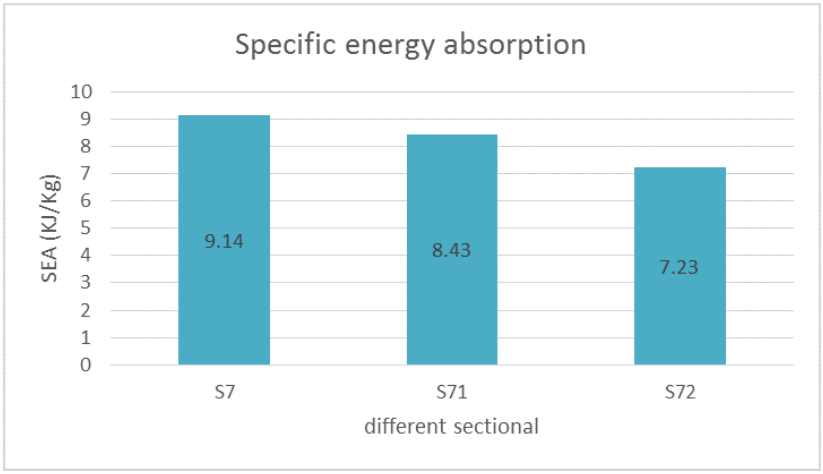

Figure 9: The results of specific energy absorption for different section configurations S_7, S_71, and S_72

on the nonlinear finite element code LS-DYNA. The results of Simulations for various sections and small hexagonal tube thicknesses t_2 are exhibited in Tables 1, 2, and 3. The TOPSIS method was used to identify the best section of small hexagonal tube thickness t_2 in three categories. The first category is t_2 = 0.4 mm, and the ratio of q is 0.25. Configuration S_6 is selected by the TOPSIS method. Comparing S_0 and S_6 demonstrated that the specific energy absorption (SEA), peak crash force (F_{max}), and crashing force efficiency (CFE) increased by 16.75, 1, and 46.1%, respectively. These results show that strengthening the aluminum single hexagonal tube with critical pick crash force can assume a $\frac{t_2}{t_1}$ of 0.25 because F_{max} increases so slowly. The results of the crashworthiness criteria for S_3 and S_4 are the same. Therefore, when the set of small hexagonal tubes rotates in the middle of the larger hexagonal tube in section S_4, the crashworthiness criteria remain unaffected. Crashworthiness criteria obtained by LS-DYNA for configuration S5 are close to the results of configurations (S_3 and S_4). The second category is t_2= 0.6 (mm), and the ratio of $\frac{t_2}{t_1}$ is 0.375. Comparing S_0 and S_7 demonstrates that SEA, F_{max}, and CFE have increased by 28.7, 10.1, and 53.5%, respectively. S_7 is the highest-ranked configuration. The third category is t_2= 0.8 (mm), and the ratio $\frac{t_2}{t_1}$ is 0.5. The best section S_7 is selected by the analysis of results for all configurations by the TOPSIS method. Comparing $S_\emptyset$ and S_7 demonstrates that SEA, Fmax, and CFE increased by 61.2, 23, and 85.8%, respectively. The results of S_3 and S_4 are the same as other categories. Therefore, the rotation of section S_3 that made S_4 does not influence

crashworthiness criteria. Afterward, semi-elliptical and semicircles with an equal circumference of straight edge size were used in the selected section S_7 when t_2=8(mm) and reduced specific energy absorption by 7.8% for section S71. Also, the SEA for section $S_7$2 decreased by approximately 20.1%, and a significant crashworthiness indicator peak force increase of 2.5% was achieved. In conclusion, the S_7 section is the best selection for multi-cell hexagonal tubes under dynamic load.

References

[1] L. Aktay, B.-H. Kröplin, A.K. Toksoy, and M. Güden, *Finite element and coupled finite element/smooth particle hydrodynamics modeling of the quasi-static crushing of empty and foam-filled single, bitubular and constraint hexagonal-and square-packed aluminum tubes*, Mater. Design **29** (2008), no. 5, 952–962.

[2] A. Alavi Nia and M.Z. Sadeghi, *The effects of foam filling on compressive response of hexagonal cell aluminum honeycombs under axial loading-experimental study*, Mater. Design **31** (2010), no. 3, 1216–1230.

[3] X. Ding, Z. Tong, Y. Liu, and S. Liu, *Dynamic axial crush analysis and design optimization of a square multi-cell thin-walled tube with lateral variable thickness*, Int. J. Mech. Sci. **140** (2018), 13–26.

[4] J. Fang, Y. Gao, G. Sun, G. Zheng, and Q. Li, *Dynamic crashing behavior of new extrudable multi-cell tubes with a functionally graded thickness*, Int. J. Mech. Sci. **103** (2015), 63–73.

[5] S. Hou, Q. Li, S. Long, X. Yang, and W. Li, *Crashworthiness design for foam filled thin-wall structures*, Mater. Design **30** (2009), no. 6, 2024–2032.

[6] S. Hunkeler, F. Duddeck, and M. Rayamajhi, *Topology optimisation method for crashworthiness design using hybrid cellular automata and thin-walled ground structures*, 9th Europ LS-DYNA Conf. Manchester, 2013.

[7] R.K. McFarland Jr, *Hexagonal cell structures under post-buckling axial load*, AIAA J. **1** (1963), no. 6, 1380–1385.

[8] Z. Pavić and V. Novoselac, *Notes on TOPSIS method*, Int. J. Res. Engin. Sci. **1** (2013), no. 2, 5–12.

[9] R. Qin, J. Zhou, and B. Chen, *Crashworthiness design and multiobjective optimization for hexagon honeycomb structure with functionally graded thickness*, Adv. Mater. Sci. Engin. **2019** (2019), 1–13.

[10] N. Qiu, Y. Gao, J. Fang, Z. Feng, G. Sun, and Q. Li, *Crashworthiness analysis and design of multi-cell hexagonal columns under multiple loading cases*, Finite Elements Anal. Design **104** (2015), 89–101.

[11] _____, *Theoretical prediction and optimization of multi-cell hexagonal tubes under axial crashing*, Thin-Walled Struct. **102** (2016), 111–121.

[12] N. Qiu, Y. Gao, J. Fang, G. Sun, and N.H. Kim, *Topological design of multi-cell hexagonal tubes under axial and lateral loading cases using a modified particle swarm algorithm*, Appl. Math. Modell. **53** (2018), 567–583.

[13] R.W. Saaty, *The analytic hierarchy process—what it is and how it is used*, Math. Modell. **9** (1987), no. 3-5, 161–176.

[14] G. Sun, T. Pang, J. Fang, G. Li, and Q. Li, *Parameterization of criss-cross configurations for multiobjective crashworthiness optimization*, Int. J. Mech. Sci. **124** (2017), 145–157.

[15] T.N. Tran, S. Hou, X. Han, and M.Q. Chau, *Crushing analysis and numerical optimization of angle element structures under axial impact loading*, Composite Struct. **119** (2015), 422–435.

[16] C.-Z. Tsai, E. Wu, and B.-H. Luo, *Forward and inverse analysis for impact on sandwich panels*, AIAA J. **36** (1998), no. 11, 2130–2136.

[17] T. Wierzbicki, *Crushing analysis of metal honeycombs*, Int. J. Impact Engin. **1** (1983), no. 2, 157–174.

[18] E. Wu and W.-S. Jiang, *Axial crush of metallic honeycombs*, Int. J. Impact Engin. **19** (1997), no. 5-6, 439–456.

[19] X.-F. Xie, W.-J. Zhang, and Z.-L. Yang, *Dissipative particle swarm optimization*, Proc. 2002 Cong. Evolut. Comput. CEC'02 (Cat. No. 02TH8600), vol. 2, IEEE, 2002, pp. 1456–1461.

[20] H. Yin, G. Wen, H. Fang, Q. Qing, X. Kong, J. Xiao, and Z. Liu, *Multiobjective crashworthiness optimization design of functionally graded foam-filled tapered tube based on dynamic ensemble metamodel*, Mater. Design **55** (2014), 747–757.

[21] H. Yin, G. Wen, S. Hou, and K. Chen, *Crushing analysis and multiobjective crashworthiness optimization of honeycomb-filled single and bitubular polygonal tubes*, Mater. Design **32** (2011), no. 8-9, 4449–4460.

[22] Z.-H. Zhan, J. Zhang, Y. Li, and H.S.-H. Chung, *Adaptive particle swarm optimization*, IEEE Trans. Syst. Man Cybernet. Part B (Cybernetics) **39** (2009), no. 6, 1362–1381.

[23] H. Zhang, X.and Zhang, *Energy absorption of multi-cell stub columns under axial compression*, Thin-Walled Struct. **68** (2013), 156–163.

[24] X. Zhang and G. Cheng, *A comparative study of energy absorption characteristics of foam-filled and multi-cell square columns*, Int. J. Impact Engin. **34** (2007), no. 11, 1739–1752.

[25] X. Zhang and H. Zhang, *Experimental and numerical investigation on crush resistance of polygonal columns and angle elements*, Thin-Walled Struct. **57** (2012), 25–36.

[26] ———, *Axial crushing of circular multi-cell columns*, Int. J. Impact Engin. **65** (2014), 110–125.

[27] G. Zhu, Q. Yu, X. Zhao, L. Wei, and H. Chen, *Energy-absorbing mechanisms and crashworthiness design of CFRP multi-cell structures*, Composite Struct. **233** (2020), 111631.